Colloid Polym Sci (2016) 294:329–337
DOI 10.1007/s00396-015-3786-2

ORIGINAL CONTRIBUTION

Fabrication and magnetic stimuli-response of polydopamine-coated core–shell structured carbonyl iron microspheres

Yu Hyun Kim[1] · **Woo Jin Ahn**[1] · **Hyoung Jin Choi**[1] · **Yongsok Seo**[2]

Received: 4 August 2015 / Revised: 29 September 2015 / Accepted: 30 September 2015 / Published online: 16 October 2015

Abstract Soft magnetic carbonyl iron (CI) for application to magnetic stimuli-responsive smart materials in an external magnetic field normally implies severe sedimentation problems because of the density imbalance between the CI particles and the dispersed medium. As a new method of ameliorating this problem, CI/polydopamine (PDA) composite particles with core–shell structure were synthesized via an oxidative self-polymerization process, bringing into an account of the coating efficiency of the PDA. Surface morphology of the CI/PDA composite particles was characterized by scanning electron microscopy, while Fourier transform infrared spectroscopy, X-ray energy-dispersive spectroscopy, and vibrating sample magnetometry were adopted to measure the chemical composition, weight and atomic percentages, and magnetic properties of the fabricated composites. The magnetic stimuli-response of their magnetorheological (MR) properties was examined by using a rotational rheometer at various magnetic field strengths and compared with pristine CI-particle-based MR fluid. The measured dynamic yield stress was fitted to a universal yield stress equation well. The sedimentation properties of the CI/PDA-composite-based MR fluid were further examined by a Turbiscan™. In addition, the anti-corrosion characteristic of these particles was also investigated.

✉ Hyoung Jin Choi
hjchoi@inha.ac.kr

✉ Yongsok Seo
ysseo@snu.ac.kr

[1] Department of Polymer Science and Engineering, Inha University, Incheon 402-751, Republic of Korea

[2] Intellectual Textiles Research Center (ITRC) and RIAM School of Materials Science and Engineering, Seoul National University, Seoul 151-744, Republic of Korea

Keywords Carbonyl iron · Polydopamine · Magnetorheological

Introduction

Magnetorheological (MR) fluids are smart materials composed of soft magnetic particles and a nonmagnetic fluid. Soft magnetic particles are more effective than hard magnetic particles in terms of their capacity to control the MR properties in response to an external field [1–4]. MR fluids show unique properties and reversibly change their phase from a liquid-like to a solid-like phase under a controlled external magnetic field [5, 6]. In the absence of a magnetic field, the behavior of MR fluids can be explained by a Newtonian fluid model, but, after applying the magnetic field, MR fluids follow a Bingham fluid model [7]. The distribution of the magnetizable particles accounts for this phenomenon: When the external magnetic field is absent, the dispersed magnetic particles are distributed randomly, but under an applied field, they form chain-like structures aligned in the direction of the magnetic field because of induced dipole–dipole interactions [8, 9]. In addition, as the applied magnetic field increases, the fluid becomes harder and more solid-like, suggesting that we can control the hardness of the MR fluid by changing the magnetic force [10]. MR fluids withstand hydrodynamic breaking by reforming the chain-like structures in the dynamic phase transition process [11, 12]. Consequently, rheological properties like the yield stress, shear viscosity, and dynamic modulus are changed [13]. Owing to these interesting characteristics, MR fluids have valuable engineering applications in active controllable shock absorbers, torque transducers, engine mounts, MR polishing devices, haptic devices, and others [14–16].

Among the numerous soft magnetic particles, carbonyl iron (CI) powder has become popular due to its high saturation magnetization, appropriate particle size, and low magnetic hysteresis [17]. However, the heavy CI particles have a density mismatch with the relatively light carrier fluids, which causes a severe sedimentation problem [18, 19]; many methods have been suggested to solve this problem. In addition, numerous magnetic materials have been explored as candidate for magneto-responsive MR materials.

Recently, several submicron-sized additives, such as clay, carbon nanofibers, carbon nanotubes, graphene oxide, or fumed silica particles, have been introduced to the CI-based MR fluid to prevent direct contact of the CI particles and improve the dispersion stability [20]. Another way to solve this problem is to coat the surface of the CI particles with polymers or inorganic materials. One of the effective ways of polymer coating is utilizing the controlled radical polymerizations [21, 22]. Through this method, the density mismatch can be reduced. [23, 24].

On the other hand, the stability against corrosion of the magnetic particles is an important factor for their long-term MR performance, because particle corrosion could deteriorate the MR efficiency [25, 26].

In this study, we developed and analyzed polymer coatings to improve the dispersion stability of the CI particles. The selected polymer was polydopamine (PDA). The major origin of the exceptionally robust adhesion is 3,4-dihydroxy-L-phenylalanine (DOPA), an analogue of dopamine. It is well known in nature that mussels have high adhesive strength to diverse substrates [27]; this strong binding strength mainly comes from the catechol group, which is one of the components of DOPA [28–30]. The oxidative self-polymerization of DOPA has the advantages of being a trouble-free, in situ process with simple elements and mild reaction conditions involving an alkaline solution at room temperature [31]. In addition, PDA has redox ability and chemical reactivity, which can be used for surface modification in various engineering fields [32–34]. The structure of catechol and the nitrogen-containing indole ring in the PDA cause the metal-binding capability [35], which makes the magnetic-particle-based PDA modification applicable to various fields such as biosensors [36], magnetism-driven precise positioning of liquid droplets [37], and a drug carrier [38].

We synthesized PDA-coated CI using a facile in situ self-oxidative polymerization under mild alkaline conditions to find a solution for the sedimentation problem of the CI-based MR fluid. PDA was polymerized at the surfaces of the CI, which consist mostly of iron; the mechanism of the surface modification with PDA has been reported previously [39, 40].

This PDA nanocomposite particle coating reduces the density of the CI particle effectively and improves the sedimentation stability. Rheological properties of MR fluids were examined by both rotational and oscillatory tests using a rotational rheometer under external magnetic fields. Dispersion stability was also examined from the sedimentation test using a Turbiscan™.

Experimental

Materials and methods

Soft magnetic carbonyl iron (CI; CC grade, density 7.87 g/cm3, BASF, Germany), silicone oil (KF-96, dynamic viscosity = 100 cS, Shin Etsu, Japan), dopamine hydrochloride (Sigma-Aldrich, USA), and Tris(hydroxymethyl)aminomethane (pH = 8.5, T&I, South Korea) were used as received.

To synthesize the CI/PDA nanocomposites, 4.5 g of CI particles was added to 900 ml of de-ionized water and ultrasonically dispersed for 30 min. Then, 12 g of 1 M Tris(hydroxymethyl)aminomethane was added to the mixture to create the weakly alkaline condition. After that, 1.8 g of dopamine hydrochloride was added and stirred for 48 h at 270 rpm at room temperature. Then, the PDA was synthesized on the surface of the CI particles by the self-oxidative polymerization process. As the reaction proceeded, the color of the dispersion changed from gray to black. After this process, the synthesized CI/PDA nanocomposite particles were washed several times with de-ionized water. Finally, the CI/PDA nanocomposite was dried under vacuum oven at 80 °C for 24 h.

Figure 1 shows a schematic diagram of synthesis process for the CI/PDA core–shell structured particles, and Fig. 1a describes the detailed reaction pathway of polymerization of dopamine. In the presence of dissolved oxygen and Tris-HCl, dopamine changes its structure to dopamine quinone. The dopamine quinone goes through a 1,4-Michael addition reaction and forms leucodopaminechrome. It then proceeds to an oxidation reaction, which produces 5,6-dihydroxyindole and indolequinone. The reverse dismutation reaction between these two states causes a polymerization reaction [31].

Soft magnetic CI particles (standard CC grade, BASF, Germany) were used as received to make a typical MR fluid system. The particles were dispersed in silicone oil (KF-96, Shin Etsu, Japan) to prepare the particle suspended MR fluid. The concentration of CI and CI/PDA was fixed to 20 vol% in both systems.

Characterization

Scanning electron microscopy (SEM; S-4300, Hitachi, Japan) characterized the morphology of the sample, and the X-ray energy-dispersive spectra coupled with Hitachi S-4200 were obtained using X-ray energy-dispersive analysis (EDAX). Fourier transform infrared (FT-IR) spectroscopy (Bruker VERTEX 80 V) was used for detection of the chemical

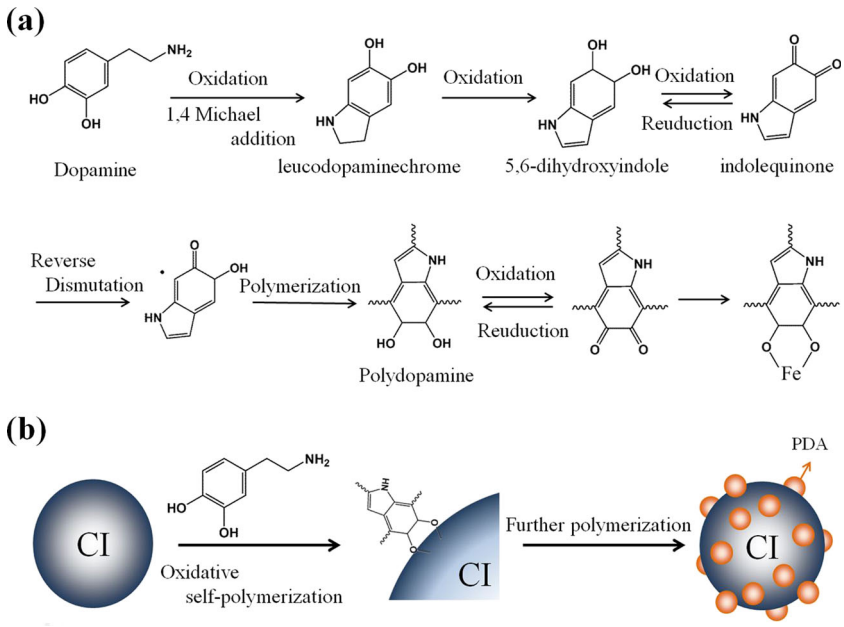

Fig. 1 **a** The detailed reaction process of polymerization of dopamine. **b** Schematic representation of synthetic process for the CI/PDA nanocomposite particles

structures of the synthesized core–shell structured composite particles. The magnetic moment of the prepared sample was characterized in powder form using a vibrating sample magnetometer (VSM; Lakeshore 7307, USA). Density of the CI/PDA particles was examined using a pycnometer. Rheological performance was characterized using a rotational rheometer (MCR300, Physica, Stuttgart, Germany) with a magnetorheological accessory (MRD 180, Physica, Stuttgart, Germany) and a 20-mm parallel plate measuring system. The measuring distance between the two parallel plates was 1 mm consistently. A Turbiscan (MA2000, Turbiscan Laboratory, France) was used to examine the sedimentation properties of the pure CI- and CI/PDA-based MR fluids.

Results and discussion

Figure 2 shows morphological images of both pure CI (Fig. 2a) and CI/PDA (Fig. 2b, c) composite particles observed with the SEM. In both cases, the particles had almost perfect spherical shape with a wide distribution of particle sizes. Before the coating process with PDA, pristine CI appeared to have a smoother surface, whereas the PDA-coated CI particles have small spherical particles on their surfaces. The densities of pristine CI and CI/PDA were characterized with a pycnometer; the measured values were 7.87 and 6.17 g/cm^3, respectively. The reduced density confirms the existence of the PDA coating on the surface of the CI particles.

Figure 2d shows the X-ray energy-dispersive spectroscopy (EDS) spectra of the CI/PDA nanocomposite. These data indicate that the synthesized material is composed of C, N, O, and Fe, confirming the existence of PDA in the composite because C (19.95 wt%), N (11.49 wt%), and O (7.93 wt%) are the elements forming the PDA structure.

Figure 3 presents the FT-IR spectra of pure CI and CI/PDA to determine the chemical structures of the PDA and CI/PDA particles. Both sample particles were mixed with KBr to make pellets and then scanned in the 400–4000 cm^{-1} wave number range. Before the measurement of the sample, baseline correction of the FT-IR apparatus was performed under vacuum at room temperature. Peaks at 1384 and 1519 cm^{-1} represent the characteristic peak of C–N–C stretching of the indole ring, and the N–H shearing vibration of the amide group, respectively. The C=C stretching vibration of the aromatic ring was detected at 1619 cm^{-1}. Each peak represents the unique chemical structures of the PDA. The FT-IR spectra of the CI/PDA possess the same unique peaks that were attributed to the PDA, confirming that the PDA was coated successfully on the surface of the CI particles.

Figure 4 gives the VSM data of both magnetic particles measured in a powder state. The magnetic moment was measured over a magnetic field ranging from −10 to 10 kOe. The large magnetization values of CI and PDA-coated CI particles were 210 and 135 emu/g, respectively, at H = 10 kOe; the particles exhibited typical soft magnetic properties with no significant hysteresis.

The MR properties of both pure CI- and CI/PDA-particle-based MR fluids were measured by a rotational rheometer in a controlled shear rate (CSR) mode; the shear rate tests were conducted in the range of 0.01–200 s^{-1}. The MR fluids were mechanically stirred for 2 min before the measurement. Figure 5 indicates that the shear stress varied as a function of the external magnetic field in the range from 0 to 343 kA/m. In the absence of an applied field, MR fluids behave like a pseudo-plastic with certain level of the yield stress. In the

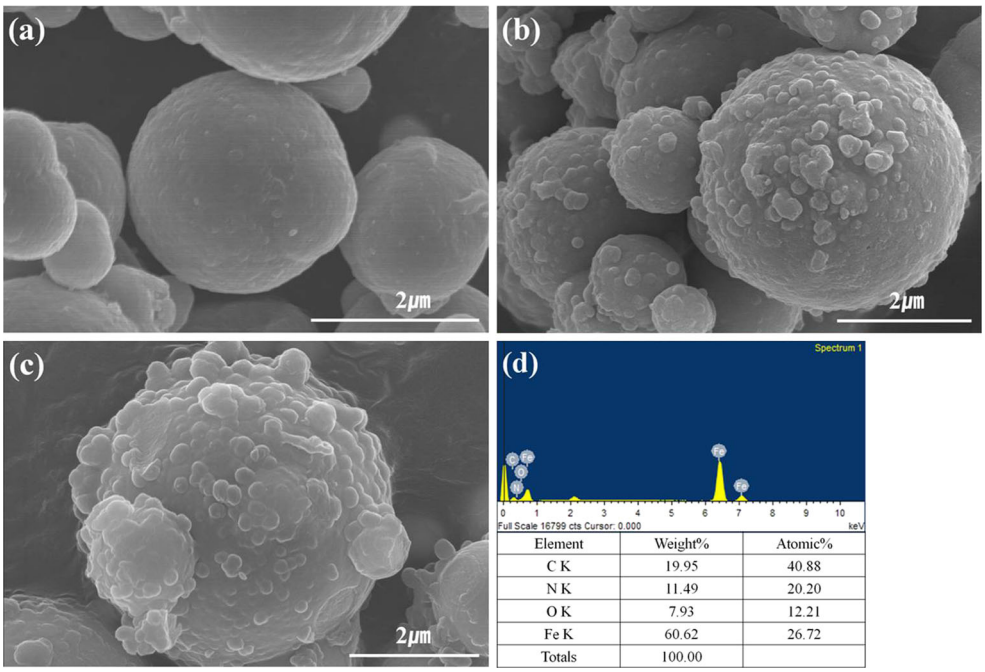

Element	Weight%	Atomic%
C K	19.95	40.88
N K	11.49	20.20
O K	7.93	12.21
Fe K	60.62	26.72
Totals	100.00	

Fig. 2 SEM images of pure CI particles (**a**) and CI/PDA (**b**, **c**), and EDS analysis (**d**) of the surface of coated particles at a point spectrum (Pt from Pt coating is removed)

presence of a magnetic field, MR fluids in general behave like a Bingham fluid [41], and the shear stress has a plateau region over a wide range of shear rate and also shows different shear stress values as the field strength changes. This can be ascribed to the formation of strong columns by virtue of the induced chain-like structures, which are driven by the robust dipole–dipole interaction between the adjoining magnetic particles [42]. This indicates that the formed structures re-form under the stable field, even though the shear deformation breaks the aligned particle cluster structures [43]. Furthermore, the yield stress of CI/PDA-based MR fluids was lower than that of pristine CI-based MR fluid. This result can be explained by the effect of the surface morphology and the resulting difference of the packing density. The morphology and coating thickness are important factors for the MR properties [44].

The flow behavior of a MR fluid can be described by applying the Bingham plastic model of Eq. (1), which is one of the most widely used models for traditional MR suspension systems, as follows: [45]

$$\begin{aligned} \tau &= \tau_y + \eta_0\,\dot{\gamma}, \quad \tau \geq \tau_y \\ \dot{\gamma} &= 0, \quad \tau < \tau_y \end{aligned} \tag{1}$$

where τ_y is the dynamic yield stress, η_0 is the post-yield viscosity, and η_0 is known to be almost equal to shear viscosity at the high shear rate [45]. The solid and dashed lines in Fig. 5 for both CI and CI/PDA suspensions were obtained from

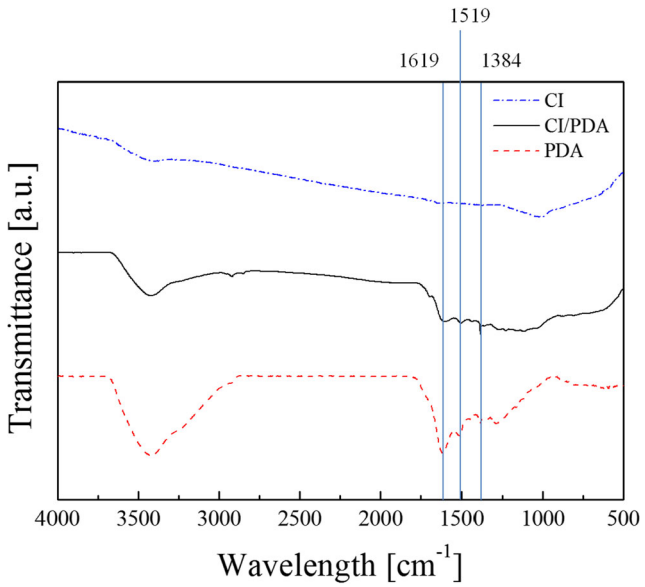

Fig. 3 FT-IR spectra of CI/PDA (*black line*) and PDA (*red line*)

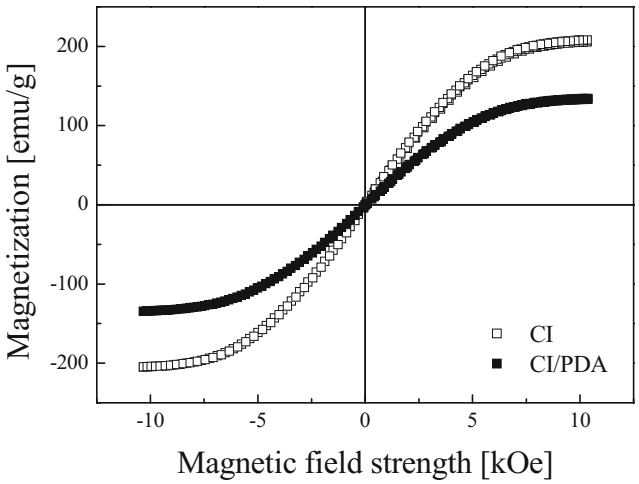

Fig. 4 Magnetization curve of CI and CI/PDA powder as a function of magnetic field strength

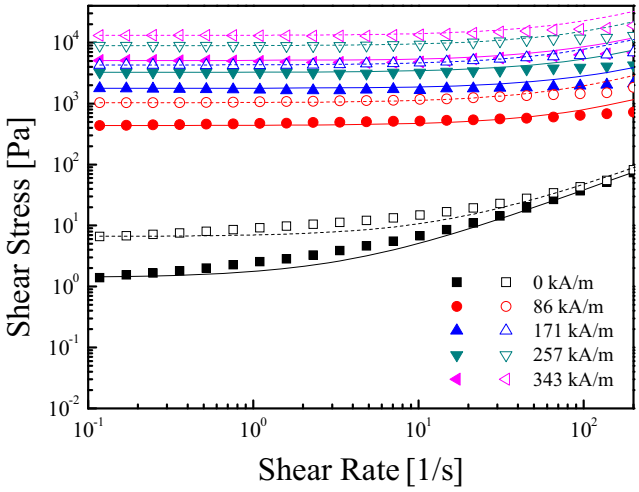

Fig. 5 Shear stress versus shear rate curves of CI/PDA (*closed symbol*) and pure CI (*open symbol*) based MR fluids

Eq. (1) and demonstrate a deviation from the experimental data. On the basis of this model, the point of dynamic yield stress could be found by extrapolating each flow curve to zero shear rate at a fixed magnetic field strength (H). The yield stress shows a very close dependency on H in a power law form $\tau_y \propto H^m$. On the other hand, the concept of a critical magnetic field strength (H_c) was proposed to measure the yield stress as a function of the applied magnetic field.

Note that for electro-rheological (ER) fluids, a universal yield stress equation has been previously proposed by adopting a critical electric field strength (E_c) [46]. Assuming the same argument in the case of a MR fluid, the new universal yield stress correlation can be described as follows:

$$\tau_y = \alpha H_0^2 \left(\frac{tanh\sqrt{H_0/H_c}}{\sqrt{H_0/H_c}} \right) \tag{4}$$

where α is relevant to the susceptibility of the fluid and volume fraction or other cognate physical parameters. τ_y has two limiting behaviors in relation to H_0, which can be expressed as follows:

$$\tau_y = \alpha H_0^2 \quad \text{for } H_0 \ll H_C, \tag{4a}$$

$$\tau_y = \alpha \sqrt{H_c} H_0^{3/2} \quad \text{for } H_0 \gg H_C, \tag{4b}$$

At low H_0, τ_y is proportional to H_0^2 as expected from the local saturation of the magnetized particles, but as the magnetic field strength reaches the intermediate range, τ_y becomes proportional to $H_0^{3/2}$. After the field strength increases enough to reach complete saturation, the particles can be treated rigorously as dipoles [47]. Both yield stress and modulus are independent of magnetic field strength, and scale with the saturation magnetization.

Figure 6 shows a log–log plot of the dynamic yield stress versus magnetic field strength for both CI- and CI/PDA-particle-based MR fluids which follows Eq. (5) well, with critical magnetic field strengths (H_c) of 204 and 196 kA/m, respectively.

A generalized scaling relationship can be obtained from Eq. (4) using H_c and $\tau_y(H_c) = 0.762\alpha H_0^2$ as follows:

$$\hat{\tau} = 1.313\hat{H}^{3/2} tanh\sqrt{\hat{H}}. \tag{5}$$

where $\hat{\tau} \equiv \tau_y(H_0) / \tau_y(H_c)$ and $\hat{H} \equiv H_0/H_C$. The data obtained from the dynamic yield stress in Fig. 6 collapse onto a single curve according to Eq. (5) as shown in Fig. 7.

Figure 8 shows the changes in shear viscosities for CI/PDA suspensions as a function of shear rate. An increase of the shear viscosity takes on an important role for controlling the properties of MR fluids. The shear viscosity was measured at four different magnetic field strengths (86, 171, 257, and 343 kA/m). When the applied magnetic field increased, the shear viscosity also increased because the external magnetic field induces a magnetic moment in the particles, which obstructs their free rotation [48]. On the other hand, each curve tends to have a shear thinning behavior independent of the existence of an external field for both CI and CI/PDA MR suspensions. This shear thinning behavior comes from changes in the internal structures under shear deformation [49, 50], implying a solid-like behavior.

Furthermore, dynamic oscillation measurement of the MR fluids was also performed using a rotating rheometer, in which before the frequency sweep, an amplitude sweep test was conducted to observe the linear viscoelastic (LVE) regions. In the LVE regions, the values of the storage modulus are independent of the strain region. The amplitude sweep test was carried out at a fixed angular frequency of 6.28 rad/s, as shown in Fig. 9. At low strain, the storage modulus has LVE regions.

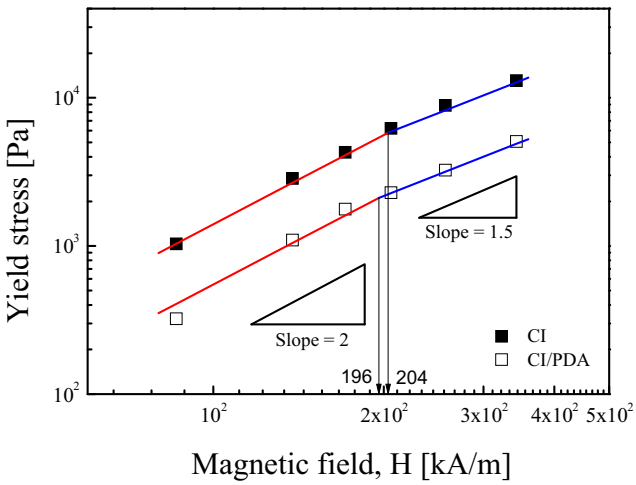

Fig. 6 Dynamic yield stress (τ_y) versus magnetic field strength (H_0) for CI and CI/PDA based MR fluids

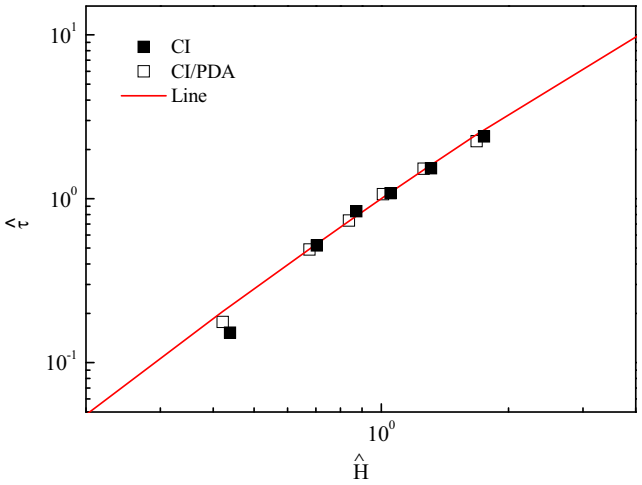

Fig. 7 Plots of $\hat{\tau}$ versus $\hat{H}$ for CI (*closed symbol*) and CI/PDA (*open symbol*) suspensions. The *solid line* is obtained from Eq. (5)

On the other hand, when excessive strain was applied, the storage modulus decreased because of irreversible changes to the structure of the MR fluids. On the basis of these results, the frequency sweeps were conducted in the LVE regions (with the strain = 0.008).

The frequency sweep was performed to examine the viscoelastic characteristics of CI/PDA-based MR fluids under different magnetic field strengths ranging from 0 to 343 kA/m. Figure 10a is frequency sweep which shows the changes of storage modulus (G′) and loss modulus (G″) as a function of angular frequency for CI/PDA suspension. The storage and loss moduli represent the elasticity and viscous behavior, respectively. At a fixed magnetic field strength, a plateau region appeared in both G′ and G″ over a wide frequency range, indicating a strong solid-like structure rather than a liquid-like structure [51]. In addition, the higher values of G′ compared to G″ were indicative of a predominantly elastic property of the CI/PDA suspension.

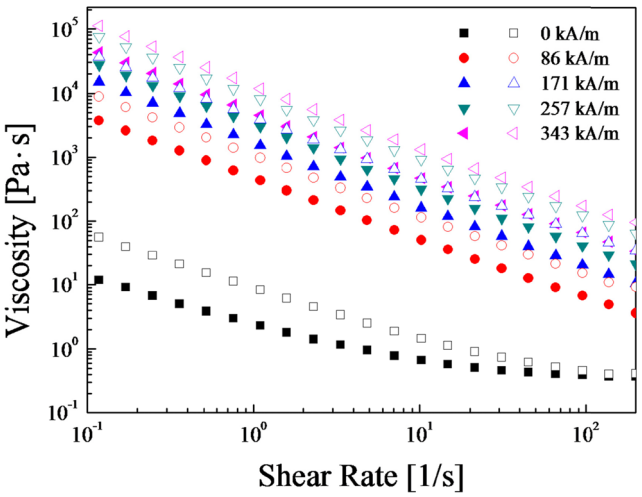

Fig. 8 Shear viscosity versus shear rate curves of CI/PDA mixture (*closed symbol*) and pure CI (*open symbol*) based MR based suspension

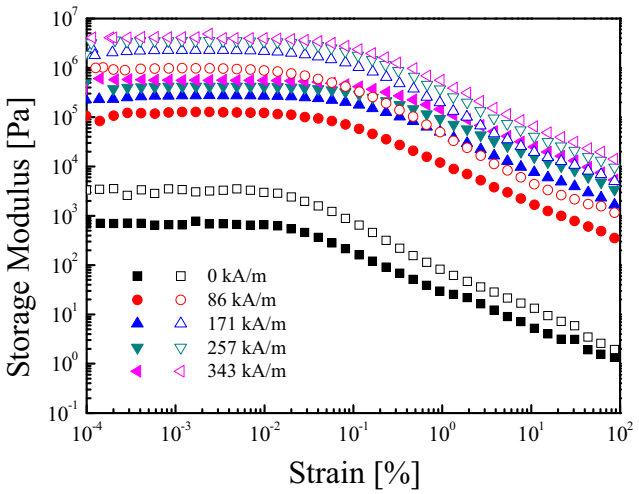

Fig. 9 Amplitude sweep CI/PDA (*closed symbol*) and CI (*open symbol*) 20 vol% MR fluids under different magnetic field strength

As shown in Fig. 10b, the CI-based MR suspension has higher value of G′ than the CI/PDA-based MR suspension

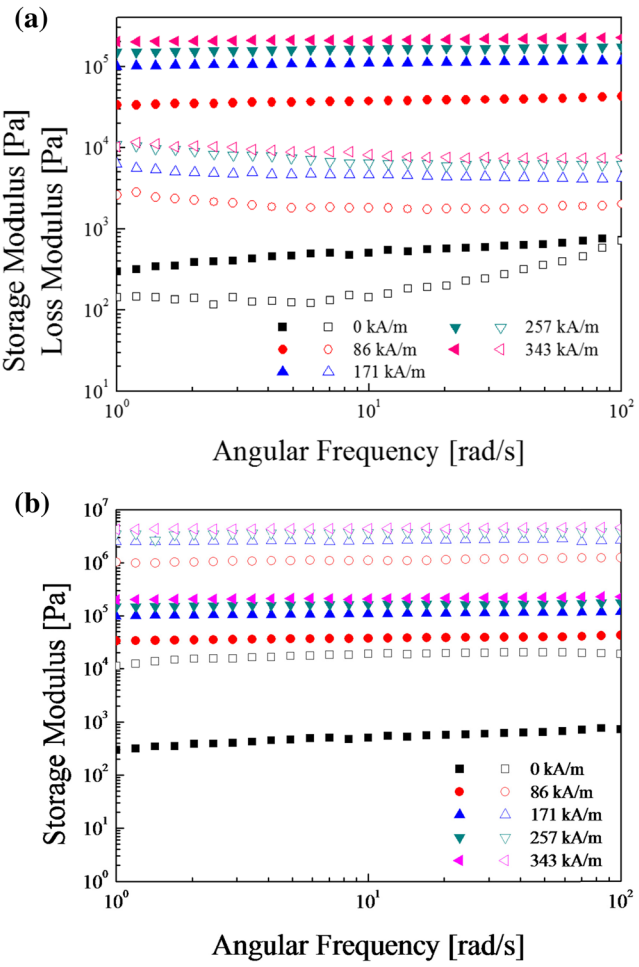

Fig. 10 **a** Frequency dependence of the storage modulus (*closed symbol*) and the loss modulus (*open symbol*) for CI/PDA suspensions and **b** storage modulus versus angular frequency of CI/PDA mixture (*closed symbol*) and pure CI (*open symbol*) based MR suspension

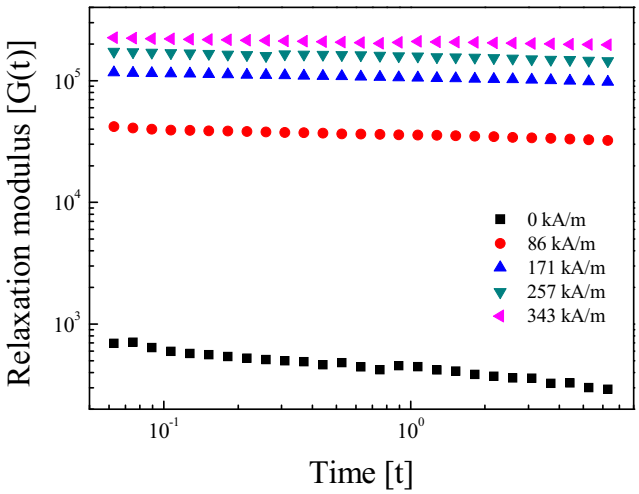

Fig. 11 Relaxation modulus G(t) of CI/PDA-based MR as calculated from G′ (ω) and G″ (ω)

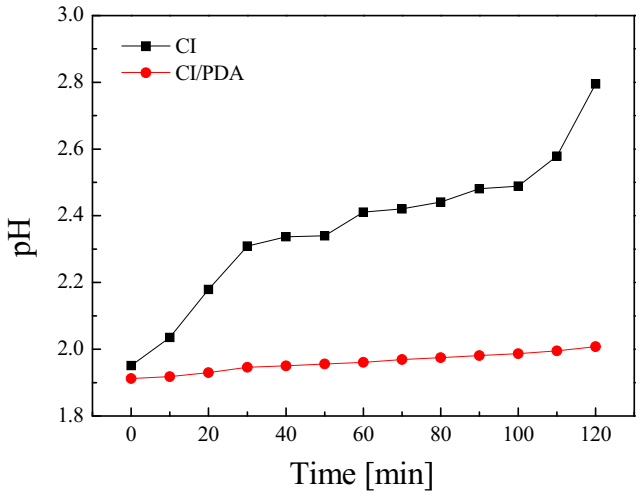

Fig. 13 Anti-acidic corrosion properties of CI and CI/PDA particles measured through pH values of dispersed particles in HCl solution

because the CI particles have superior magnetic properties compared with those of the CI/PDA systems.

The stress relaxation behavior is one way to confirm the phase change in MR fluids from a liquid-like to a solid-like phase. Figure 11 demonstrates stress relaxation behavior, in which the stress relaxation modulus was calculated by using the values of G′ (ω) and G″ (ω) in Fig. 10a, along with Eq. (6), which is the common formula known as the Schwarzl equation [52, 53]:

$$G(t) \cong G'(\omega) - 0.560G''(\omega/2) + 0.200G''(\omega) \quad (6)$$

The $G(t)$ becomes linear on a log–log scale in the presence of external magnetic fields and increases with higher magnetic field strength. This result suggests that there are strong interactions among the CI/PDA particles under the magnetic fields [54], making their solid-like characteristics.

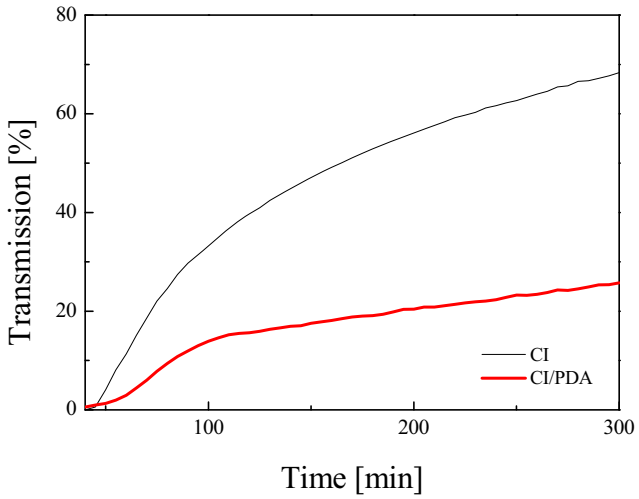

Fig. 12 Turbiscan spectra of pure CI-based MR fluid and CI/PDA based MR fluid

The sedimentation phenomenon of both CI- and CI/PDA-based MR fluids was examined with a Turbiscan, which uses a multiple light scattering technique to measure the destabilizing phenomena in suspension systems. A Turbiscan sensor consists of two synchronous detectors and a pulsed near-infrared light source at 880 nm. The transmission detector measures the light emerging from the sample at 0° from the incident beam [55]. As shown in Fig. 12, CI/PDA-based MR suspensions have better dispersion stability than pure CI-based MR suspensions; this can be explained by the reduced density mismatch between the oil medium and the particles. Compared with a previous study of PGMA-coated CI particle with a density of 6.96 g/cm^3 [56], the CI/PDA-based MR fluids exhibit improved sedimentation stability.

Furthermore, the stability against anti-acidic corrosion was investigated and compared for both pure CI and CI/PDA particles. The pH values of both particles were measured in HCl solution as a function of time, which can be shown in Fig. 13. A rapid increase of the pH value of the CI-HCl solution was observed, indicating that the reaction occurred between the CI powder and the acid. On the contrary, a flat line of the pH value is shown in the CI/PDA-HCl solution system. This result indicates that the PDA coating improved the anti-acidic corrosion stability of the CI particles.

Conclusion

As a novel method to fabricate organic–inorganic hybrids that provide enhanced dispersion stability, PDA-coated CI particles for MR fluids were synthesized via an in situ self-oxidative polymerization. After coating, the density of the particles decreased, suggesting a more stable dispersion ability of CI/PDA-based MR fluids than those using pristine CI particles. The morphology of these particles was confirmed by

SEM. The VSM results showed a decrease of magnetic moment after PDA coating. The MR properties were measured via steady shear and frequency sweep testing using a rotational rheometer and compared with pure CI-based MR fluid. Even though the MR properties exhibited lower shear stress than the pristine CI-based MR fluid, typical MR behavior was well-preserved in both the shear and frequency sweep tests. The dispersion stability was examined using a Turbiscan. The MR suspension composed of PDA-coated CI has an improved sedimentation rate due to the reduced density mismatch. Anti-corrosion characteristics of these particles were investigated by comparing their pH values measured in HCl solution as a function of time.

Acknowledgments This research was supported by Ministry of Trade, Industry & Energy, Republic of Korea (# 10047791).

References

1. Andrei OE, Bica I (2009) Some mechanisms concerning the electrical conductivity of magnetorheological suspensions in magnetic field. J Ind Eng Chem 15:573–577
2. Margida AJ, Weiss KD, Carlson JD (1996) Magnetorheological materials based on iron alloy particles. Int J Mod Phys B 10:3335–3341
3. de Vicente J, Klingenberg DJ, Hidalgo-Alvarez R (2011) Magnetorheological fluids: a review. Soft Matter 7:3701–3710
4. Pacull J, Goncalves S, Delgado AV, Duran JDG, Jimenez ML (2009) Effect of polar interactions on the magnetorheology of silica-coated magnetite suspensions in oil media. J Colloid Interf Sci 337:254–259
5. Bica I (2002) Damper with magnetorheological suspension. J Magn Magn Mater 241:196–200
6. Dodbiba G, Park HS, Okaya K, Fujita T (2008) Investigating magnetorheological properties of a mixture of two types of carbonyl iron powders suspended in an ionic liquid. J Magn Magn Mater 320:1322–1327
7. Bossis G, Khuzir P, Lacis S, Volkova O (2003) Yield behavior of magnetorheological suspensions. J Magn Magn Mater 258: 456–458
8. Rankin PJ, Ginder JM, Klingenberg DJ (1998) Electro- and magneto-rheology. Curr Opin Colloid Interf 3:373–381
9. Bica I, Anitas EM, Averis LME, Bunoiu M (2015) Magnetodielectric effects in composite materials based on paraffin, carbonyl iron and graphene. J Ind Eng Chem 21:1323–1327
10. Sherman SG, Wereley NM (2013) Effect of particle size distribution on chain structures in magnetorheological fluids. IEEE Trans Magn 49:3430–3433
11. Felicia LJ, Philip J (2013) Probing of field-induced structures and tunable rheological properties of surfactant capped magnetically polarizable nanofluids. Langmuir 29:110–120
12. An HN, Groenewold J, Picken SJ, Mendes E (2014) Conformational changes of a single magnetic particle string within gels. Soft Matter 10:997–1005
13. Hong CH, Liu YD, Choi HJ (2013) Carbonyl iron suspension with halloysite additive and its magnetorheology. Appl Clay Sci 80–81: 366–371
14. Hu W, Cook E, Wereley NM (2007) Energy absorber using a magnetorheological bypass valve filled with ferromagnetic beads. IEEE Trans Magn 43:2695–2697
15. Bica I (2009) Influence of magnetic field upon the electric capacity of a flat capacitor having magnetorheological elastomer as a dielectric. J Ind Eng Chem 15:605–609
16. Yang TH, Koo JH, Kim SY, Kyung KU, Kwon DS (2012) Application of magnetorheological fluids for a miniature haptic button: Experimental evaluation. J Intel Mater Syst Str 23: 1025–1031
17. de Vicente J, Lopez-Lopez MT, Gonzalez-Caballero F, Duran JDG (2003) Rheological study of the stabilization of magnetizable colloidal suspensions by addition of silica nanoparticles. J Rheol 47: 1093–1109
18. Wu WP, Zhao BY, Wu Q, Chen LS, Hu KA (2006) The strengthening effect of guar gum on the yield stress of magnetorheological fluid. Smart Mater Struct 15:N94–N98
19. Ngatu GT, Wereley NM (2007) Viscometric and sedimentation characterization of bidisperse magnetorheological fluids. IEEE Trans Magn 43:2474–2476
20. Fang FF, Jang IB, Choi HJ (2007) Single-walled carbon nanotube added carbonyl iron suspension and its magnetorheology. Diam Relat Mater 16:1167–1169
21. Hu B, Fuchs A, Huseyin S, Gordaninejad F, Evrensel C (2006) Atom transfer radical polymerized MR fluids. Polymer 47: 7653–7663
22. Cvek M, Mrlik M, Ilcikova M, Plachy T, Sedlacik M, Mosnacek J, Pavlinek V (2015) A facile controllable coating of carbonyl iron particles with poly(glycidyl methacrylate): a tool for adjusting MR response and stability properties. J Mater Chem C 3:4646–4656
23. Machovsky M, Mrlik M, Kuritka I, Pavlinek V, Babayan V (2014) Novel synthesis of core-shell urchin-like ZnO coated carbonyl iron microparticles and their magnetorheological activity. RSC Adv 4: 996–1003
24. Bombard AJF, Knobel M, Alcantara MR (2007) Phosphate coating on the surface of carbonyl iron powder and its effect in magnetorheological suspensions. Int J Mod Phys B 21:4858–4867
25. Pu H, Jiang F, Wang Y, Yan B (2010) Soft magnetic composite particles of reduced iron coated with poly(p-xylylene) via chemical vapor deposition polymerization. Colloids Surf A 361:62–65
26. Mrlik M, Ilcikova M, Sedlacik M, Mosnacek J, Peer P, Filip P (2014) Cholesteryl-coated carbonyl iron particles with improved anti-corrosion stability and their viscoelastic behavior under magnetic field. Colloid Polym Sci 292:2137–2143
27. Liu YL, Ai KL, Lu LH (2014) Polydopamine and its derivative materials: synthesis and promising applications in energy, environmental, and biomedical fields. Chem Rev 114: 5057–5115
28. Dalsin JL, Hu BH, Lee BP, Messersmith PB (2003) Mussel adhesive protein mimetic polymers for the preparation of nonfouling surfaces. J Am Chem Soc 125:4253–4258
29. Lee H, Dellatore SM, Miller WM, Messersmith PB (2007) Mussel-inspired surface chemistry for multifunctional coatings. Science 318:426–430
30. Statz AR, Meagher RJ, Barron AE, Messersmith PB (2005) New peptidomimetic polymers for antifouling surfaces. J Am Chem Soc 127:7972–7973
31. An P, Zuo F, Li XH, Wu YP, Zhang JH, Zheng ZH, Ding XB, Peng YX (2013) A bio-inspired polydopamine approach to preparation of gold-coated Fe_3O_4 core-shell nanoparticles: synthesis, characterization and mechanism. Nano 8:1350061
32. Zhang YW, Zhang Y, Wang H, Shen GL, Yu RQ (2009) Fabrication of a novel enzyme immobilization platform using bio-mimetic dopamine polymer films and nanogold particles. Acta Chim Sinica 67: 2375–2380
33. Sureshkumar M, Siswanto DY, Lee CK (2010) Magnetic antimicrobial nanocomposite based on bacterial cellulose and silver nanoparticles. J Mater Chem 20:6948–6955

34. Fei B, Qian BT, Yang ZY, Wang RH, Liu WC, Mak CL, Xin JH (2008) Coating carbon nanotubes by spontaneous oxidative polymerization of dopamine. Carbon 46:1795–1797
35. Wang WC, Jiang Y, Wen SP, Liu L, Zhang LQ (2012) Preparation and characterization of polystyrene/Ag core-shell microspheres—a bio-inspired poly(dopamine) approach. J Colloid Interf Sci 368: 241–249
36. Peng HP, Liang RP, Zhang L, Qiu JD (2013) Facile preparation of novel core-shell enzyme-Au-polydopamine-Fe3O4 magnetic bionanoparticles for glucose sensor. Biosens Bioelectron 42: 293–299
37. Yang FC, Dong Y, Guo ZG (2014) Facile fabrication of core shell Fe3O4@polydopamine microspheres with unique features of magnetic control behavior and special wettability. Colloid Surf A 463: 101–109
38. Liu R, Guo YL, Odusote G, Qu FL, Priestley RD (2013) Core-shell Fe_3O_4 polydopamine nanoparticles serve multipurpose as drug carrier, catalyst support and carbon adsorbent. ACS Appl Mater Interfaces 5:9167–9171
39. Yu F, Chen SG, Chen Y, Li HM, Yang L, Chen YY, Yin YS (2010) Experimental and theoretical analysis of polymerization reaction process on the polydopamine membranes and its corrosion protection properties for 304 Stainless Steel. J Mol Struct 982:152–161
40. Wilker JJ (2010) Marine bioinorganic materials: mussels pumping iron. Curr Opin Chem Biol 14:276–283
41. de Vicente J, Lopez-Lopez MT, Duran JDG, Gonzalez-Caballero F (2004) Shear flow behavior of confined magnetorheological fluids at low magnetic field strengths. Rheol Acta 44:94–103
42. Tian Y, Jiang JL, Meng YG, Wen SZ (2010) A shear thickening phenomenon in magnetic field controlled-dipolar suspensions. Appl Phys Lett 97:151904
43. Mrlik M, Ilcikova M, Pavlinek V, Mosnacek J, Peer P, Filip P (2013) Improved thermooxidation and sedimentation stability of covalently-coated carbonyl iron particles with cholesteryl groups and their influence on magnetorheology. J Colloid Interf Sci 396: 146–151
44. Park BJ, Fang FF, Zhang K, Choi HJ (2010) Polymer-coated magnetic carbonyl iron microparticles and their magnetorheological characteristics. Korean J Chem Eng 27:716–722
45. Wereley NM, Chaudhuri A, Yoo JH, John S, Kotha S, Suggs A, Radhakrishnan R, Love BJ, Sudarshan TS (2006) Bidisperse magnetorheological fluids using Fe particles at nanometer and micron scale. J Intel Mat Syst Str 17:393–401
46. Choi HJ, Cho MS, Kim JW, Kim CA, Jhon MS (2001) A yield stress scaling function for electrorheological fluids. Appl Phys Lett 78:3806–3808
47. Ginder JM, Davis LC, Elie LD (1996) Rheology of magnetorheological fluids: models and measurements. Int J Mod Phys B 10:3293–3303
48. Hato MJ, Choi HJ, Sim HH, Park BO, Ray SS (2011) Magnetic carbonyl iron suspension with organoclay additive and its magnetorheological properties. Colloid Surf A 377:103–109
49. Cho MS, Lim ST, Jang IB, Choi HJ, Jhon MS (2004) Encapsulation of spherical iron-particle with PMMA and its magnetorheological particles. IEEE Trans Magn 40:3036–3038
50. Fang FF, Choi HJ, Seo Y (2010) Sequential coating of magnetic carbonyl iron particles with polystyrene and multiwalled carbon nanotubes and its effect on their magnetorheology. ACS Appl Mater Interfaces 2:54–60
51. Gandhi F, Bullough WA (2005) On the phenomenological modeling of electrorheological and magnetorheological fluid preyield behavior. J Intel Mat Syst Str 16:237–248
52. Park BJ, Kim TH, Choi HJ, Lee JH (2007) Emulsion polymerized polystyrene/montmorillonite nanocomposite and its viscoelastic characteristics. J Macromol Sci B 46:341–354
53. Schwarzl FL (1975) Numerical calculation of stress relaxation modulus from dynamic data for linear viscoelastic materials. Rheol Acta 14:581–590
54. Zhang WL, Choi HJ (2012) Silica-graphene oxide hybride composite particles and their electroresponsive characteristics. Langmuir 28:7055–7062
55. Fang FF, Liu YD, Choi HJ, Seo YS (2011) Core-shell structured carbonyl iron microspheres prepared via dual-step functionality coatings and their magnetorheological response. ACS Appl Mater Interfaces 3:3487–3495
56. Kim SY, Kwon SH, Liu YD, Lee JS, You CY, Choi HJ (2014) Core–shell-structured cross-linked poly(glycidyl methacrylate)-coated carbonyl iron microspheres and their magnetorheology. J Mater Sci 49:1345–1352